Energy Compression and Stabilization of Laser-Plasma Accelerators

A. Ferran Pousa,[1,*] I. Agapov,[1] S. A. Antipov,[1] R. W. Assmann,[1,2] R. Brinkmann,[1] S. Jalas,[3] M. Kirchen,[1] W. P. Leemans,[1,3] A. R. Maier,[1] A. Martinez de la Ossa,[1] J. Osterhoff,[1] and M. Thévenet[1]

[1] *Deutsches Elektronen-Synchrotron DESY, Notkestr. 85, 22607 Hamburg, Germany*
[2] *Laboratori Nazionali di Frascati, Via Enrico Fermi 40, 00044 Frascati, Italy*
[3] *Department of Physics Universität Hamburg, Luruper Chaussee 149, 22761 Hamburg, Germany*

(Dated: September 6, 2022)

Laser-plasma accelerators outperform current radiofrequency technology in acceleration strength by orders of magnitude. Yet, enabling them to deliver competitive beam quality for demanding applications, particularly in terms of energy spread and stability, remains a major challenge. In this Letter, we propose to combine bunch decompression and active plasma dechirping for drastically improving the energy profile and stability of beams from laser-plasma accelerators. Realistic start-to-end simulations demonstrate the potential of these post-acceleration phase-space manipulations for simultaneously reducing an initial energy spread and energy jitter of ∼1–2 % to ≲0.1 %, closing the beam-quality gap to conventional acceleration schemes.

Laser-plasma accelerators (LPAs) [1] can give rise to a new generation of ultra-compact particle accelerators with a wide range of applications. Among others, they could enable cost-effective coherent light sources [2, 3] or injectors for storage rings [4, 5]. Improvements in beam quality such as the demonstration of peaked energy spectra [6–8], GeV energy [9–11], high current [12] and low emittance [13–15], bring the performance of these devices closer to that of radiofrequency (RF) accelerators. Still, challenges limiting their applicability remain, particularly regarding the beam energy spread and stability.

Applications such as free-electron lasers (FELs) require an energy spread ≲0.1 % [16], yet current LPAs typically operate in the ∼1 % range [17]. The main source behind this is typically the steep slope of the accelerating fields, which leads to beams with a strong longitudinal energy correlation (chirp), together with various contributions to the slice energy spread [18–20]. Many techniques have been proposed for reducing the energy chirp of plasma beams, either within the acceleration stage [21–23] or in a dedicated external device [24–31]. A promising approach is the use of beam loading [32–34] for flattening the average accelerating gradient along the LPA [35–38]. This has enabled the demonstration of the first sub-percent energy spread beams capable of generating FEL radiation [3]. Nonetheless, reaching the performance of conventional machines demands further improvements to the energy spread as well as to the shot-to-shot energy jitter, which currently ranges in the few percent [3, 17].

The energy stability is critical for the beam transport downstream of the LPA, and thus for virtually any application. Especially demanding is the injection into diffraction-limited storage rings, where particle energy deviations up to ∼1 % [39] are tolerated. This requires an energy jitter and energy spread ≲0.1 % rms. Recent developments in machine learning and active feedback loops [37, 40, 41] offer a path towards LPAs of improved stability, particularly with the onset of kilohertz lasers [42–44], but a permille energy jitter is yet to be demonstrated.

In this Letter, we propose a technique for drastically – and simultaneously – reducing the energy spread and energy jitter of LPA beams in a two-step process. First, longitudinal decompression in a magnetic chicane is used to imprint a linear correlation between the particles' arrival time and energy [23, 45–48]. Second, a linear longitudinal electric field is applied to remove the imprinted correlation and correct deviations with respect to the target energy. This is carried out by an *active* plasma dechirper (APD), a dedicated plasma stage where the wakefields are generated by a fraction of the LPA driver. In contrast to *passive* plasma dechirpers [24–27], where the wakefields are generated by the electron beam itself, an APD takes advantage of the intrinsic synchronization between the LPA and APD drivers for correcting the central energy jitter, and not only the energy spread. This combination of chicane and APD is the first demonstration of a plasma-based energy compression system [49, 50]. Its working principle resembles that of chirped-pulse amplification in lasers [51]. Realistic start-to-end simulations show that this method can be incorporated into state-of-the-art LPAs [36, 37] for improving the energy spread and stability by an order of magnitude, closing the performance gap to RF accelerators.

The combined effect of decompression and dechirping can be studied by investigating the single-particle dynamics. By establishing a reference energy γ_{ref} as the desired beam energy of the accelerator, a relative energy deviation $\delta(t) = (\gamma(t) - \gamma_{\mathrm{ref}})/\gamma_{\mathrm{ref}}$ and longitudinal coordinate $\zeta(t) = z(t) - z_{\mathrm{ref}}(t)$ can be defined for each particle. Here, $\gamma = \sqrt{1 + (\mathbf{p}/m_e c)^2}$ is the relativistic Lorentz factor, with $\mathbf{p}$ and m_e being, respectively, the momentum and rest mass of an electron; c is the speed of light in vacuum; t is time; z is the longitudinal position; and z_{ref} is the position of a reference particle with $\delta = 0$ initially located at the beam center. A dispersive section transforms the phase-space coordinates of a particle initially at $(\zeta_i,\, \delta_i)$ to a final position $\zeta_f = \zeta_i + R_{56}\delta_i + \mathcal{O}(\delta_i^2)$ [53], where R_{56} is the linear dispersion coefficient, while leav-

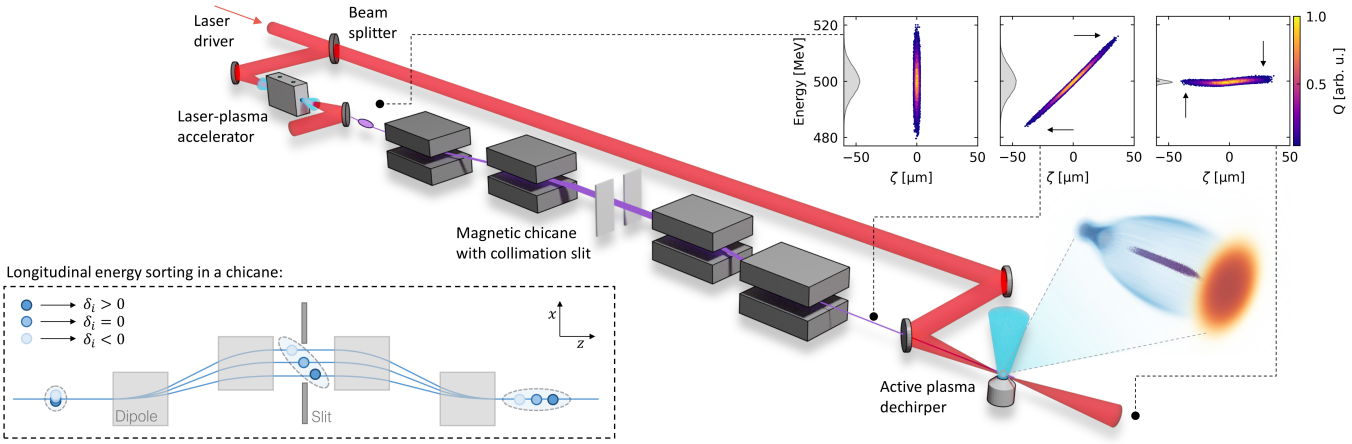

FIG. 1. Basic layout and working principle of an LPA energy compressor and stabilizer. Only the LPA source and the relevant beam line components (laser, chicane and APD) are shown. The longitudinal phase space of the beam at different locations is also displayed, as well as the 3D [52] wakefield structure in the APD.

ing the energy unchanged. Thus, to first order in δ_i, a beam with no initial correlation between ζ_i and δ_i is longitudinally stretched by a factor

$$S \equiv \frac{\sigma_{\zeta_f}}{\sigma_{\zeta_i}} = \sqrt{\left(\frac{R_{56}\sigma_{\delta_i}}{\sigma_{\zeta_i}}\right)^2 + 1}\ , \tag{1}$$

while developing a linear chirp $\chi \equiv \sigma_{\zeta\delta}/\sigma_\zeta^2 = R_{56}^{-1}(1 - S^{-2})$, which is $\chi \simeq R_{56}^{-1}$ for $S^2 \gg 1$. Here, σ_ζ and σ_δ are the standard deviations of ζ and δ, and $\sigma_{\zeta\delta}$ is their covariance. After decompression, the beam enters a dechirper of length L that applies a linear longitudinal electric field $E_z(\zeta) = -(m_e c^2/e)\,\mathcal{E}'\,(\zeta - \zeta_0)$ with normalized slope $\mathcal{E}'$ centered at ζ_0, where e is the elementary charge. Assuming a highly relativistic beam ($\gamma \gg 1$), ζ_f stays constant throughout the dechirper and the particle energy is transformed into a final value

$$\delta_f = \frac{1}{R_{56}}(\zeta_f - \zeta_i) + \frac{\mathcal{E}' L}{\gamma_{\rm ref}}(\zeta_f - \zeta_0)\ . \tag{2}$$

Therefore, the energy correlation imprinted by the linear dispersion can be removed by the dechirper if

$$\mathcal{E}' L = -\frac{\gamma_{\rm ref}}{R_{56}}\ . \tag{3}$$

This results in a net reduction of the beam energy spread, whose final value is fully determined by R_{56} as

$$\sigma_{\delta_f} = \frac{\sigma_{\zeta_i}}{R_{56}} \simeq \frac{\sigma_{\delta_i}}{S}\ , \tag{4}$$

where the last equality holds if $S^2 \gg 1$.

This technique is ideally suited for LPA beams. As Eq. (4) shows, the typically ultra-short (∼1 µm) length and large (∼1 %) energy spread allow for a factor 10 decompression and energy spread reduction with minimal dispersion ($R_{56} \sim 1$ mm). In addition, the high initial peak current (up to ∼10 kA [12]) means that a final current in the ∼1 kA range can still be achieved after decompression, allowing for FEL applications. When high current is not required, such as in storage ring injectors, an even more drastic energy spread reduction could be realized.

As illustrated in Fig. 1, the bunch decompression can be performed by a magnetic chicane, where path length differences arise due to an energy-dependent transverse deflection. This results in $R_{56} = 2\theta^2(L_d + 2L_m/3)$ [53], where L_m and θ are, respectively, the magnet length and bending angle (for $\delta = 0$); and L_d is the distance between the central and outer dipoles.

When Eq. (3) is satisfied, Eq. (2) also yields that the final deviation of the average beam energy is given by

$$\langle \delta_f \rangle = \frac{\zeta_0}{R_{56}}\ . \tag{5}$$

Therefore, if $\zeta_0 = 0$, the final beam energy is stabilized to $\gamma_{\rm ref}$ regardless of its initial value. This requires the ability to control ζ_0 independently of the beam position, i.e., with an *active* dechirping medium where the fields are not generated by the beam itself. An APD accomplishes this in a compact, plasma-based setup. It is conceptually similar to a laser-plasma lens [54, 55], but aimed at the generation of longitudinal, instead of transverse, fields with a fraction of the LPA driver. The intrinsic synchronization between the LPA and APD drivers allows for a precise control of ζ_0, independently of the electron beam arrival time. This setup is also robust against realistic timing jitters between both drivers. As obtained from Eq. (5), if $R_{56} \sim 1$ mm, a state-of-the-art timing jitter of $\lesssim$10 fs [56, 57] is sufficient for achieving a per-mille energy jitter.

When the peak normalized vector potential of the APD driver is sufficiently high (i.e, $a_0 \gtrsim 2$), large plasma electron cavitation occurs and a trailing wakefield with uniform $\mathcal{E}'$ is generated (cf. Fig 2(a)). The length of the

cavity is approximately given by the plasma wavelength $\lambda_p = 2\pi/k_p$, where $k_p = (n_p e^2/m_e\epsilon_0 c^2)^{1/2}$ and n_p are the plasma electron wavenumber and density and ϵ_0 is the vacuum permittivity. As depicted in Fig. 1, a slit in the center of the chicane removes particles beyond a maximum, $\delta_{\max}$, and minimum, $\delta_{\min}$, energy deviation for ensuring that the stretched beam fits within the cavity. Imposing a total beam extension $\lesssim\lambda_p/2$ yields the condition $\lambda_p \gtrsim 2\,(\delta_{\max} - \delta_{\min})R_{56} = 2\,(\delta_{\max} - \delta_{\min})\sigma_{\zeta_i}/\sigma_{\delta_f}$, which determines the maximum plasma density for achieving a certain final energy spread. For $\sigma_{\delta_f} = 10^{-3}$, $\sigma_{\zeta_i} = 1\,\mu\text{m}$ and $\delta_{\max} - \delta_{\min} = 0.06$, $n_p \lesssim 8\times10^{16}\,\text{cm}^{-3}$ is obtained. The field slope $\mathcal{E}'$ can be estimated from the non-linear cold fluid equation [58] for the wakefield potential, ψ, behind the driver, i.e., $\mathcal{E}'(\zeta) = \partial_\zeta^2\psi(\zeta) = -k_p^2\,(1-1/(1+\psi(\zeta))^2)/2$. At ζ_0, which occurs around the center of the cavity, ψ is maximum and given approximately by $\psi_0 \equiv \psi(\zeta_0) \sim \hat{w}_0^2/4$ [59], where $\hat{w}_0 = k_p w_0$ and w_0 is the spot size of the laser at focus. This implies that $\mathcal{E}'(\zeta_0) \sim -k_p^2\,(1 - 1/(1+\hat{w}_0^2/4)^2)/2$. Coupled with Eq. (3), this expression allows for an estimate of the required APD length, under the assumption that $w \sim w_0$ throughout the dechirper. Relative to the laser Rayleigh length, $Z_R = \pi w_0^2/\lambda_0$ [58], the APD length is found to be $L/Z_R = 2\gamma_{\text{ref}}\lambda_0\,(4+\hat{w}_0^2)^2/(\pi R_{56}\hat{w}_0^4(8+\hat{w}_0^2))$, where λ_0 is the laser wavelength. For $R_{56} = 1\,\text{mm}$, $\gamma_{\text{ref}} = 10^3$ and $\lambda_0 = 800\,\text{nm}$, this expression yields $\hat{w}_0 \gtrsim 1$ for ensuring $L \lesssim Z_R$ (i.e. $w \sim w_0$). Under this condition, a compact, mm-long APD can be realized without external laser guiding. Given the typically low density and narrow driver, no self-injection and, thus, no dark current is expected from the APD [60, 61].

The performance of the technique is demonstrated by means of two comprehensive simulation studies of an energy compression system. First, the setup is probed with an ideal Gaussian electron bunch to generally assess the energy spread and jitter correction. Second, a full start-to-end study including a realistic LPA and relevant experimental jitters validates its efficacy under real-world conditions. The initial beam capture and final focus into the APD are carried out by active plasma lenses [62]. This enables a compact setup with minimal chromatic emittance growth [63], but other options are also possible [5, 64]. After initial prototyping with `Wake-T` [65], the plasma elements are simulated with the quasi-3D particle-in-cell code `FBPIC` [66] and the conventional elements with `Ocelot` [67], including the effects of 3D space charge and 1D coherent synchrotron radiation (CSR). Using `libEnsemble` [68], the jitter of the setup is comprehensively evaluated with hundreds of simulations. See [69] for additional simulation details.

The parameters of the probe Gaussian electron beam are representative of current state-of-the-art LPAs [3, 36–38], having a 500 MeV energy with 1 % rms shot-to-shot jitter, 1 % rms energy spread, 1 µm normalized emittance, 2 µm transverse size, 0.5 mrad rms divergence, 10 fs FWHM duration, and 10 pC charge. The chicane has a total length of 2 m, with $L_d = 50\,\text{cm}$, $L_m = 20\,\text{cm}$ and $\theta = 34.4\,\text{mrad}$, resulting in $R_{56} = 1.5\,\text{mm}$ and $S = 11.8$. It includes a collimating slit with a 1.4 mm horizontal aperture for filtering particles with $|\delta| > 3\,\%$. The APD has a 6.8 mm plateau with a $3.2\times10^{16}\,\text{cm}^{-3}$ density and two 0.3 mm Gaussian ramps at the entrance and exit. The APD driver is a 2 J Gaussian laser pulse focused at the center of the plateau with $a_0 = 2.15$, $\lambda_0 = 0.8\,\mu\text{m}$, $w_0 = 22\,\mu\text{m}$, and a 25 fs FWHM duration. The plasma lenses have a 1 cm length, $1.62\,\text{kT}\,\text{m}^{-1}$ focusing gradient, and $10^{15}\,\text{cm}^{-3}$ density. They are placed 10 cm down and upstream of the initial beam and the APD, respectively.

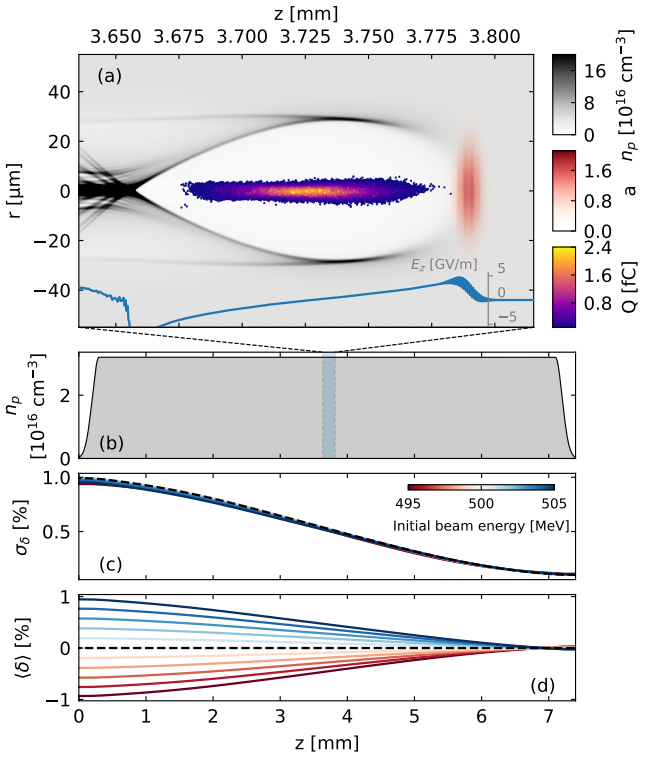

FIG. 2. (a) Plasma wakefields and electron beam at the center of the APD. (b) APD density profile. (c) Energy spread and (d) average energy deviation along the APD of beams with initial energy deviations between ±1 %. The black dashed line corresponds to a reference initial energy of 500 MeV.

Fig. 2 shows the evolution of the decompressed Gaussian beam within the APD for initial energy deviations between ±1 %. The wakefields generated by the driver effectively reduce the energy spread while simultaneously correcting the initial energy deviations. The reference beam has a final energy spread of ∼0.10 % (total) and ∼0.084 % (slice average). This agrees with Eq. (4), which predicts a value of ∼0.085 %. The total energy spread is larger due to non-linearities in E_z arising mostly from beam loading. The efficacy of the energy compression can be clearly seen in Fig. 3. The results from 300 simu-

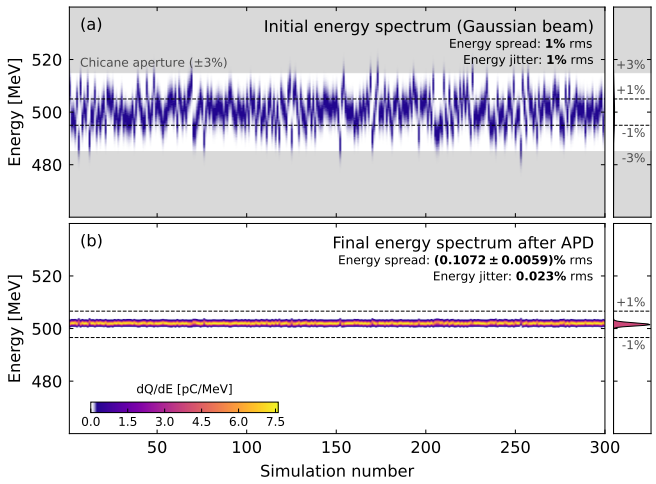

FIG. 3. (a) Initial energy spectrum of 300 Gaussian beams with a 1 % rms energy jitter and energy spread. The gray area represents the energies filtered out by the slit in the chicane. (b) Final energy spectrum after the APD.

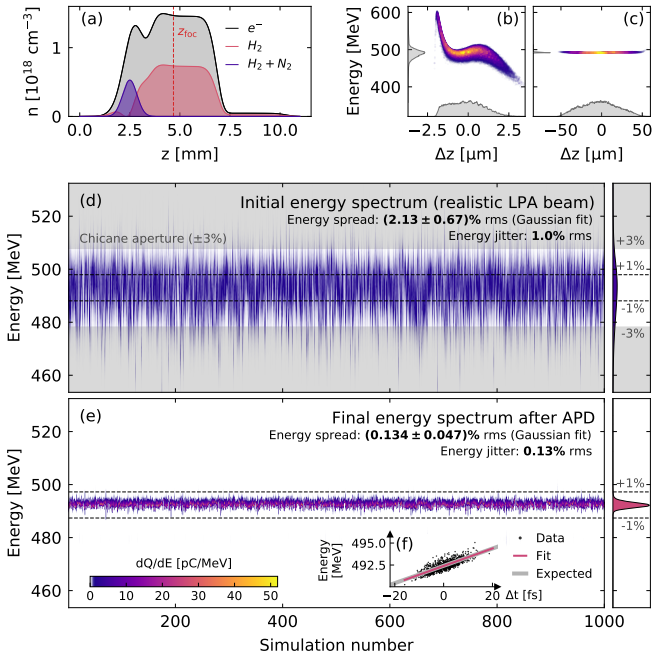

FIG. 4. Results from the start-to-end jitter study: (a) LPA density profile; longitudinal phase space of the reference beam (i.e., no jitters) at the exit of the (b) LPA and (c) APD; beam energy spectra at the (d) LPA and (e) APD exits; (f) average beam energy versus laser arrival time jitter (Δt), including the expected correlation and a linear fit to the data.

lations show that the initial energy jitter of 1 % is reduced to 0.023 %. Similarly, the initial energy spread of 1 % is reduced by a factor ∼10 to (0.1072 ± 0.0059) %. The final normalized emittances of (1.22 ± 0.13) µm (horizontal) and (1.179 ± 0.086) µm (vertical) show only a slight increase dominated by chromatic effects during capture and focus. These values correspond to the average and rms deviations of all simulated shots. Ultimately, this study demonstrates that the energy compressor behaves as expected from theory, improving the energy spread and stability by at least an order of magnitude.

The real-world applicability of the energy compressor is validated through a full start-to-end study including a realistic LPA as well as relevant experimental jitters. The LPA used for this study is based on downramp-assisted ionization injection, a well-proven technique which can be accurately simulated [36, 37] and where the dominant sources of jitter are well known: laser focal position, energy, and pulse duration [17, 36]. It is designed as an evolution of the LUX target [17, 36, 37] aimed at generating 500 MeV beams with maximum stability to laser jitters. The density profile, displayed in Fig. 4(a), contains a mixture of H_2 and N_2 (1 %) for electron injection, a 1.46×10^{18} cm^{-3} plateau for acceleration, and a low-density tail (4×10^{16} cm^{-3}) for divergence minimization [69]. The laser driver is a 130 TW Ti:Sa system with a total energy of 4.68 J, split between the LPA (2.68 J) and the APD (2 J). Its longitudinal profile is Gaussian with a FWHM duration of 34 fs, while its transverse profile is modeled as a so-called flattened Gaussian [70]. This consists of a sum of Laguerre-Gauss modes that accurately describes flat-top high-power lasers in experiments [71]. The laser is subject to realistic jitters in the focal plane position (100 µm rms), energy (0.5 % rms) and pulse duration (1 % rms) [36, 72]. Transverse and longitudinal (i.e., timing) jitters between the LPA and APD pulses of 5 µm [71] and 5 fs rms, respectively, are also included at the APD entrance. The LPA driver is focused to $w_0 = 21$ µm, with $a_0 = 2.21$, at $z_{\rm foc} = 4.68$ mm into the target. The data from 1000 simulations shows that the resulting LPA beams have an energy of (494.3 ± 4.9) MeV (i.e., 1 % jitter), an rms (Gaussian fit) energy spread of (2.13 ± 0.67) %, a normalized emittance of (2.48 ± 0.12) µm (horizontal) and (0.749 ± 0.062) µm (vertical), a divergence of (0.762 ± 0.026) mrad (horizontal) and (0.350 ± 0.029) mrad (vertical), a charge of (49.8 ± 5.6) pC, a FWHM duration of (8.96 ± 0.57) fs and a peak current of (5.63 ± 0.87) kA. A realistic pointing jitter of 0.5 mrad, consistent with experiments [36], is externally added. To transport this beam, the focusing gradient in the first and second plasma lenses is tuned to 1.60 kT m^{-1} and 2.37 kT m^{-1}, respectively. The APD is placed 6.6 cm downstream of the second lens and has a 5.4 mm plateau with a 4.1×10^{16} cm^{-3} density. The laser driver is focused at the center of the APD with $w_0 = 27.5$ µm and $a_0 = 1.48$.

The results of this jitter scan can be seen in Fig. 4. After the APD, the beams have an average energy of (492.41 ± 0.63) MeV (i.e., 0.13 % jitter) and an rms (Gaussian fit) energy spread of (0.134 ± 0.047) % (total) and (0.071 ± 0.012) % (slice). This is an order of magni-

tude improvement over the initial values, and demonstrates a dechirping strength of $\sim 62\,\mathrm{GeV\,mm^{-1}\,m^{-1}}$, a factor $>10^3$ higher than with RF technology [5]. The final energy variability is dominated by the timing jitter between the two laser pulses. This can be seen in Fig. 4(f), where the observed time-energy correlation is in full agreement with Eq. (5). The final beam emittances of $(5.4 \pm 1.2)\,\mu\mathrm{m}$ (horizontal) and $(1.78 \pm 0.85)\,\mu\mathrm{m}$ (vertical) experience an increase mostly due to chromatic effects in the transport line and transverse offsets of the laser at the APD entrance, which also lead to an increased pointing jitter of 1.91 mrad (horizontal) and 1.84 mrad (vertical). The final beam charge of $(34.8 \pm 5.6)\,\mathrm{pC}$ is reduced due to the collimating slit in the chicane, resulting in a peak current of $(0.180 \pm 0.038)\,\mathrm{kA}$ for a bunch duration of $(193 \pm 46)\,\mathrm{fs}$. This study demonstrates the feasibility and robustness of the proposed concept under real-world conditions, paving the way towards the experimental demonstration of reliable and high-quality plasma accelerators. Side effects such as emittance growth or charge loss can be greatly minimized by a lower initial energy spread, and the final energy stability can be further improved if the laser timing jitter is reduced.

In conclusion, the presented concept of bunch decompression and active plasma dechirping effectively corrects the energy spread and jitter of LPAs in a compact setup. Large-scale realistic start-to-end simulations demonstrate that the beam energy spread and energy jitter of state-of-the-art LPAs can be reduced by an order of magnitude to the permille and sub-permille range. This would enable LPAs as compact beam sources for future storage rings or free-electron lasers.

We thank R. Lehe for providing access to the optimization library used to fine-tune the APD parameters in the presented studies. This research was supported in part through the Maxwell computational resources operated at Deutsches Elektronen-Synchrotron DESY, Hamburg, Germany. The authors gratefully acknowledge the Gauss Centre for Supercomputing e.V. (www.gauss-centre.eu) for funding this project by providing computing time through the John von Neumann Institute for Computing (NIC) on the GCS Supercomputer JUWELS [73] at Jülich Supercomputing Centre (JSC).

* angel.ferran.pousa@desy.de

[1] T. Tajima and J. M. Dawson, Laser electron accelerator, Phys. Rev. Lett. **43**, 267 (1979).

[2] K. Nakajima, Towards a table-top free-electron laser, Nat. Phys. **4**, 92 (2008).

[3] W. Wang, K. Feng, L. Ke, C. Yu, Y. Xu, R. Qi, Y. Chen, Z. Qin, Z. Zhang, M. Fang, J. Liu, K. Jiang, H. Wang, C. Wang, X. Yang, F. Wu, Y. Leng, J. Liu, R. Li, and Z. Xu, Free-electron lasing at 27 nanometres based on a laser wakefield accelerator, Nature **595**, 516 (2021).

[4] S. Hillenbrand, R. Assmann, A.-S. Müller, O. Jansen, V. Judin, and A. Pukhov, Study of laser wakefield accelerators as injectors for synchrotron light sources, Nucl. Instrum. Methods Phys. Res. A **740**, 153 (2014), proceedings of the first European Advanced Accelerator Concepts Workshop 2013.

[5] S. A. Antipov, A. Ferran Pousa, I. Agapov, R. Brinkmann, A. R. Maier, S. Jalas, L. Jeppe, M. Kirchen, W. P. Leemans, A. M. de la Ossa, J. Osterhoff, M. Thévenet, and P. Winkler, Design of a prototype laser-plasma injector for an electron synchrotron, Phys. Rev. Accel. Beams **24**, 111301 (2021).

[6] S. P. D. Mangles, C. D. Murphy, Z. Najmudin, A. G. R. Thomas, J. L. Collier, A. E. Dangor, E. J. Divall, P. S. Foster, J. G. Gallacher, C. J. Hooker, D. A. Jaroszynski, A. J. Langley, W. B. Mori, P. A. Norreys, F. S. Tsung, R. Viskup, B. R. Walton, and K. Krushelnick, Monoenergetic beams of relativistic electrons from intense laser–plasma interactions, Nature **431**, 535 (2004).

[7] C. G. R. Geddes, C. Toth, J. van Tilborg, E. Esarey, C. B. Schroeder, D. Bruhwiler, C. Nieter, J. Cary, and W. P. Leemans, High-quality electron beams from a laser wakefield accelerator using plasma-channel guiding, Nature **431**, 538 (2004).

[8] J. Faure, Y. Glinec, A. Pukhov, S. Kiselev, S. Gordienko, E. Lefebvre, J.-P. Rousseau, F. Burgy, and V. Malka, A laser–plasma accelerator producing monoenergetic electron beams, Nature **431**, 541 (2004).

[9] W. P. Leemans, B. Nagler, A. J. Gonsalves, C. Tóth, K. Nakamura, C. G. R. Geddes, E. Esarey, C. B. Schroeder, and S. M. Hooker, Gev electron beams from a centimetre-scale accelerator, Nat. Phys. **2**, 696 (2006).

[10] W. P. Leemans, A. J. Gonsalves, H.-S. Mao, K. Nakamura, C. Benedetti, C. B. Schroeder, C. Tóth, J. Daniels, D. E. Mittelberger, S. S. Bulanov, J.-L. Vay, C. G. R. Geddes, and E. Esarey, Multi-gev electron beams from capillary-discharge-guided subpetawatt laser pulses in the self-trapping regime, Phys. Rev. Lett. **113**, 245002 (2014).

[11] A. J. Gonsalves, K. Nakamura, J. Daniels, C. Benedetti, C. Pieronek, T. C. H. de Raadt, S. Steinke, J. H. Bin, S. S. Bulanov, J. van Tilborg, C. G. R. Geddes, C. B. Schroeder, C. Tóth, E. Esarey, K. Swanson, L. Fan-Chiang, G. Bagdasarov, N. Bobrova, V. Gasilov, G. Korn, P. Sasorov, and W. P. Leemans, Petawatt laser guiding and electron beam acceleration to 8 gev in a laser-heated capillary discharge waveguide, Phys. Rev. Lett. **122**, 084801 (2019).

[12] O. Lundh, J. Lim, C. Rechatin, L. Ammoura, A. Ben-Ismaïl, X. Davoine, G. Gallot, J.-P. Goddet, E. Lefebvre, V. Malka, and J. Faure, Few femtosecond, few kiloampere electron bunch produced by a laser–plasma accelerator, Nat. Phys. **7**, 219 (2011).

[13] S. Fritzler, E. Lefebvre, V. Malka, F. Burgy, A. E. Dangor, K. Krushelnick, S. P. D. Mangles, Z. Najmudin, J.-P. Rousseau, and B. Walton, Emittance measurements of a laser-wakefield-accelerated electron beam, Phys. Rev. Lett. **92**, 165006 (2004).

[14] E. Brunetti, R. P. Shanks, G. G. Manahan, M. R. Islam, B. Ersfeld, M. P. Anania, S. Cipiccia, R. C. Issac, G. Raj, G. Vieux, G. H. Welsh, S. M. Wiggins, and D. A. Jaroszynski, Low emittance, high brilliance relativistic electron beams from a laser-plasma accelerator,

Phys. Rev. Lett. **105**, 215007 (2010).
[15] R. Weingartner, S. Raith, A. Popp, S. Chou, J. Wenz, K. Khrennikov, M. Heigoldt, A. R. Maier, N. Kajumba, M. Fuchs, B. Zeitler, F. Krausz, S. Karsch, and F. Grüner, Ultralow emittance electron beams from a laser-wakefield accelerator, Phys. Rev. ST Accel. Beams **15**, 111302 (2012).
[16] S. Corde, K. Ta Phuoc, G. Lambert, R. Fitour, V. Malka, A. Rousse, A. Beck, and E. Lefebvre, Femtosecond x rays from laser-plasma accelerators, Rev. Mod. Phys. **85**, 1 (2013).
[17] A. R. Maier, N. M. Delbos, T. Eichner, L. Hübner, S. Jalas, L. Jeppe, S. W. Jolly, M. Kirchen, V. Leroux, P. Messner, M. Schnepp, M. Trunk, P. A. Walker, C. Werle, and P. Winkler, Decoding sources of energy variability in a laser-plasma accelerator, Phys. Rev. X **10**, 031039 (2020).
[18] C. Lin, J. van Tilborg, K. Nakamura, A. J. Gonsalves, N. H. Matlis, T. Sokollik, S. Shiraishi, J. Osterhoff, C. Benedetti, C. B. Schroeder, C. Tóth, E. Esarey, and W. P. Leemans, Long-range persistence of femtosecond modulations on laser-plasma-accelerated electron beams, Phys. Rev. Lett. **108**, 094801 (2012).
[19] A. Ferran Pousa, A. Martinez de la Ossa, and R. W. Assmann, Intrinsic energy spread and bunch length growth in plasma-based accelerators due to betatron motion, Sci. Rep. **9**, 17690 (2019).
[20] X. Li, P. A. P. Nghiem, and A. Mosnier, Toward low energy spread in plasma accelerators in quasilinear regime, Phys. Rev. Accel. Beams **21**, 111301 (2018).
[21] R. Brinkmann, N. Delbos, I. Dornmair, M. Kirchen, R. Assmann, C. Behrens, K. Floettmann, J. Grebenyuk, M. Gross, S. Jalas, T. Mehrling, A. Martinez de la Ossa, J. Osterhoff, B. Schmidt, V. Wacker, and A. R. Maier, Chirp mitigation of plasma-accelerated beams by a modulated plasma density, Phys. Rev. Lett. **118**, 214801 (2017).
[22] G. G. Manahan, A. F. Habib, P. Scherkl, P. Delinikolas, A. Beaton, A. Knetsch, O. Karger, G. Wittig, T. Heinemann, Z. M. Sheng, J. R. Cary, D. L. Bruhwiler, J. B. Rosenzweig, and B. Hidding, Single-stage plasma-based correlated energy spread compensation for ultrahigh 6d brightness electron beams, Nat. Commun. **8**, 15705 (2017).
[23] A. Ferran Pousa, A. Martinez de la Ossa, R. Brinkmann, and R. W. Assmann, Compact multistage plasma-based accelerator design for correlated energy spread compensation, Phys. Rev. Lett. **123**, 054801 (2019).
[24] R. D'Arcy, S. Wesch, A. Aschikhin, S. Bohlen, C. Behrens, M. J. Garland, L. Goldberg, P. Gonzalez, A. Knetsch, V. Libov, A. M. de la Ossa, M. Meisel, T. J. Mehrling, P. Niknejadi, K. Poder, J.-H. Röckemann, L. Schaper, B. Schmidt, S. Schröder, C. Palmer, J.-P. Schwinkendorf, B. Sheeran, M. J. V. Streeter, G. Tauscher, V. Wacker, and J. Osterhoff, Tunable plasma-based energy dechirper, Phys. Rev. Lett. **122**, 034801 (2019).
[25] V. Shpakov, M. P. Anania, M. Bellaveglia, A. Biagioni, F. Bisesto, F. Cardelli, M. Cesarini, E. Chiadroni, A. Cianchi, G. Costa, M. Croia, A. Del Dotto, D. Di Giovenale, M. Diomede, M. Ferrario, F. Filippi, A. Giribono, V. Lollo, M. Marongiu, V. Martinelli, A. Mostacci, L. Piersanti, G. Di Pirro, R. Pompili, S. Romeo, J. Scifo, C. Vaccarezza, F. Villa, and A. Zigler, Longitudinal phase-space manipulation with beam-driven plasma wakefields, Phys. Rev. Lett. **122**, 114801 (2019).
[26] Y. P. Wu, J. F. Hua, Z. Zhou, J. Zhang, S. Liu, B. Peng, Y. Fang, Z. Nie, X. N. Ning, C.-H. Pai, Y. C. Du, W. Lu, C. J. Zhang, W. B. Mori, and C. Joshi, Phase space dynamics of a plasma wakefield dechirper for energy spread reduction, Phys. Rev. Lett. **122**, 204804 (2019).
[27] Y. P. Wu, J. F. Hua, C.-H. Pai, W. An, Z. Zhou, J. Zhang, S. Liu, B. Peng, Y. Fang, S. Y. Zhou, X. L. Xu, C. J. Zhang, F. Li, Z. Nie, W. Lu, W. B. Mori, and C. Joshi, Near-ideal dechirper for plasma-based electron and positron acceleration using a hollow channel plasma, Phys. Rev. Applied **12**, 064011 (2019).
[28] S. Antipov, S. Baturin, C. Jing, M. Fedurin, A. Kanareykin, C. Swinson, P. Schoessow, W. Gai, and A. Zholents, Experimental demonstration of energy-chirp compensation by a tunable dielectric-based structure, Phys. Rev. Lett. **112**, 114801 (2014).
[29] F. Mayet, R. Assmann, and F. Lemery, Longitudinal phase space synthesis with tailored 3d-printable dielectric-lined waveguides, Phys. Rev. Accel. Beams **23**, 121302 (2020).
[30] K. Bane and G. Stupakov, Corrugated pipe as a beam dechirper, Nucl. Instrum. Methods Phys. Res. A **690**, 106 (2012).
[31] F. Fu, R. Wang, P. Zhu, L. Zhao, T. Jiang, C. Lu, S. Liu, L. Shi, L. Yan, H. Deng, C. Feng, Q. Gu, D. Huang, B. Liu, D. Wang, X. Wang, M. Zhang, Z. Zhao, G. Stupakov, D. Xiang, and J. Zhang, Demonstration of nonlinear-energy-spread compensation in relativistic electron bunches with corrugated structures, Phys. Rev. Lett. **114**, 114801 (2015).
[32] S. van der Meer, Improving the power efficiency of the plasma wakefield accelerator, CERN Tech. Report No. PS-85-65-AA, CLIC-Note-3 (1985).
[33] M. Tzoufras, W. Lu, F. S. Tsung, C. Huang, W. B. Mori, T. Katsouleas, J. Vieira, R. A. Fonseca, and L. O. Silva, Beam loading in the nonlinear regime of plasma-based acceleration, Phys. Rev. Lett. **101**, 145002 (2008).
[34] K. V. Lotov, Efficient operating mode of the plasma wakefield accelerator, Phys. Plasmas **12**, 053105 (2005).
[35] J. P. Couperus, R. Pausch, A. Köhler, O. Zarini, J. M. Krämer, M. Garten, A. Huebl, R. Gebhardt, U. Helbig, S. Bock, K. Zeil, A. Debus, M. Bussmann, U. Schramm, and A. Irman, Demonstration of a beam loaded nanocoulomb-class laser wakefield accelerator, Nat. Commun. **8**, 487 (2017).
[36] M. Kirchen, S. Jalas, P. Messner, P. Winkler, T. Eichner, L. Hübner, T. Hülsenbusch, L. Jeppe, T. Parikh, M. Schnepp, and A. R. Maier, Optimal beam loading in a laser-plasma accelerator, Phys. Rev. Lett. **126**, 174801 (2021).
[37] S. Jalas, M. Kirchen, P. Messner, P. Winkler, L. Hübner, J. Dirkwinkel, M. Schnepp, R. Lehe, and A. R. Maier, Bayesian optimization of a laser-plasma accelerator, Phys. Rev. Lett. **126**, 104801 (2021).
[38] L. T. Ke, K. Feng, W. T. Wang, Z. Y. Qin, C. H. Yu, Y. Wu, Y. Chen, R. Qi, Z. J. Zhang, Y. Xu, X. J. Yang, Y. X. Leng, J. S. Liu, R. X. Li, and Z. Z. Xu, Near-gev electron beams at a few per-mille level from a laser wakefield accelerator via density-tailored plasma, Phys. Rev. Lett. **126**, 214801 (2021).
[39] C. G. Schroer, R. Roehlsberger, E. Weckert, R. Wanzen-

berg, I. Agapov, R. Brinkmann, and W. Leemans, *PETRA IV: upgrade of PETRA III to the Ultimate 3D X-ray microscope. Conceptual Design Report* (Deutsches Elektronen-Synchrotron DESY, Hamburg, 2019).

[40] S. J. D. Dann, C. D. Baird, N. Bourgeois, O. Chekhlov, S. Eardley, C. D. Gregory, J.-N. Gruse, J. Hah, D. Hazra, S. J. Hawkes, C. J. Hooker, K. Krushelnick, S. P. D. Mangles, V. A. Marshall, C. D. Murphy, Z. Najmudin, J. A. Nees, J. Osterhoff, B. Parry, P. Pourmoussavi, S. V. Rahul, P. P. Rajeev, S. Rozario, J. D. E. Scott, R. A. Smith, E. Springate, Y. Tang, S. Tata, A. G. R. Thomas, C. Thornton, D. R. Symes, and M. J. V. Streeter, Laser wakefield acceleration with active feedback at 5 hz, Phys. Rev. Accel. Beams **22**, 041303 (2019).

[41] R. J. Shalloo, S. J. D. Dann, J.-N. Gruse, C. I. D. Underwood, A. F. Antoine, C. Arran, M. Backhouse, C. D. Baird, M. D. Balcazar, N. Bourgeois, J. A. Cardarelli, P. Hatfield, J. Kang, K. Krushelnick, S. P. D. Mangles, C. D. Murphy, N. Lu, J. Osterhoff, K. Põder, P. P. Rajeev, C. P. Ridgers, S. Rozario, M. P. Selwood, A. J. Shahani, D. R. Symes, A. G. R. Thomas, C. Thornton, Z. Najmudin, and M. J. V. Streeter, Automation and control of laser wakefield accelerators using bayesian optimization, Nat. Commun. **11**, 6355 (2020).

[42] Z.-H. He, B. Hou, V. Lebailly, J. A. Nees, K. Krushelnick, and A. G. R. Thomas, Coherent control of plasma dynamics, Nat. Commun. **6**, 7156 (2015).

[43] Z.-H. He, B. Hou, G. Gao, V. Lebailly, J. A. Nees, R. Clarke, K. Krushelnick, and A. G. R. Thomas, Coherent control of plasma dynamics by feedback-optimized wavefront manipulation, Phys. Plasmas **22**, 056704 (2015).

[44] D. Gustas, D. Guénot, A. Vernier, S. Dutt, F. Böhle, R. Lopez-Martens, A. Lifschitz, and J. Faure, High-charge relativistic electron bunches from a khz laser-plasma accelerator, Phys. Rev. Accel. Beams **21**, 013401 (2018).

[45] C. M. S. Sears, E. Colby, R. J. England, R. Ischebeck, C. McGuinness, J. Nelson, R. Noble, R. H. Siemann, J. Spencer, D. Walz, T. Plettner, and R. L. Byer, Phase stable net acceleration of electrons from a two-stage optical accelerator, Phys. Rev. ST Accel. Beams **11**, 101301 (2008).

[46] A. R. Maier, A. Meseck, S. Reiche, C. B. Schroeder, T. Seggebrock, and F. Grüner, Demonstration scheme for a laser-plasma-driven free-electron laser, Phys. Rev. X **2**, 031019 (2012).

[47] F. Mayet, R. W. Aßmann, R. Brinkmann, J. Bödewadt, U. Dorda, W. Kuropka, C. Lechner, B. Marchetti, and J. Zhu, A concept for phase-synchronous acceleration of microbunch trains in dla structures at sinbad, in *Proceedings of 8th International Particle Accelerator Conference (IPAC'17)*, edited by V. R. W. Schaa, G. Arduini, J. Pranke, M. Seidel, and M. Lindroos (JACoW Publishing, Geneva, Switzerland, 2017).

[48] A. Ferran Pousa, R. Assmann, R. Brinkmann, and A. Martinez de la Ossa, External injection into a laser-driven plasma accelerator with sub-femtosecond timing jitter, J. Phys. Conf. Ser. **874**, 012032 (2017).

[49] W. A. Gillespie and M. G. Kelliher, The energy compressor at the glasgow 170 mev electron linac, Nucl. Instrum. Methods **184**, 285 (1981).

[50] P. Piot, D. R. Douglas, and G. A. Krafft, Longitudinal phase space manipulation in energy recovering linac-driven free-electron lasers, Phys. Rev. ST Accel. Beams **6**, 030702 (2003).

[51] D. Strickland and G. Mourou, Compression of amplified chirped optical pulses, Opt. Commun. **55**, 447 (1985).

[52] A. Ferran Pousa, R. W. Assmann, and A. Martinez de la Ossa, VisualPIC: A New Data Visualizer and Post-Processor for Particle-in-Cell Codes, in *Proceedings of 8th International Particle Accelerator Conference (IPAC'17)*, edited by V. R. W. Schaa, G. Arduini, J. Pranke, M. Seidel, and M. Lindroos (JACoW Publishing, Geneva, Switzerland, 2017).

[53] A. W. Chao, K. H. Mess, M. Tigner, and F. Zimmermann, eds., *Handbook of accelerator physics and engineering* (World Scientific, Hackensack, USA, 2013) p. 335.

[54] R. Lehe, C. Thaury, E. Guillaume, A. Lifschitz, and V. Malka, Laser-plasma lens for laser-wakefield accelerators, Phys. Rev. ST Accel. Beams **17**, 121301 (2014).

[55] C. Thaury, E. Guillaume, A. Döpp, R. Lehe, A. Lifschitz, K. Ta Phuoc, J. Gautier, J.-P. Goddet, A. Tafzi, A. Flacco, F. Tissandier, S. Sebban, A. Rousse, and V. Malka, Demonstration of relativistic electron beam focusing by a laser-plasma lens, Nat. Commun. **6**, 6860 (2015).

[56] S. Schulz, I. GrguraÅ¡, C. Behrens, H. Bromberger, J. T. Costello, M. K. Czwalinna, M. Felber, M. C. Hoffmann, M. Ilchen, H. Y. Liu, T. Mazza, M. Meyer, S. Pfeiffer, P. PrÄ™dki, S. Schefer, C. Schmidt, U. Wegner, H. Schlarb, and A. L. Cavalieri, Femtosecond all-optical synchronization of an x-ray free-electron laser, Nat. Commun. **6**, 5938 (2015).

[57] R. Shalloo, C. Arran, G. Cheung, L. Corner, J. Holloway, R. Walczak, S. Hooker, N. Booth, O. Chekhlov, C. Gregory, *et al.*, Measurement of femtosecond-scale drift and jitter of the delay between the north and south beams of gemini, Central Laser Facility Annual Report , 36 (2015).

[58] E. Esarey, C. B. Schroeder, and W. P. Leemans, Physics of laser-driven plasma-based electron accelerators, Rev. Mod. Phys. **81**, 1229 (2009).

[59] W. Lu, C. Huang, M. Zhou, M. Tzoufras, F. S. Tsung, W. B. Mori, and T. Katsouleas, A nonlinear theory for multidimensional relativistic plasma wave wakefields, Phys. Plasmas **13**, 056709 (2006).

[60] C. B. Schroeder, E. Esarey, B. A. Shadwick, and W. P. Leemans, Trapping, dark current, and wave breaking in nonlinear plasma waves, Phys. Plasmas **13**, 033103 (2006).

[61] I. Kostyukov, A. Pukhov, and S. Kiselev, Phenomenological theory of laser-plasma interaction in "bubble" regime, Phys. Plasmas **11**, 5256 (2004).

[62] J. van Tilborg, S. Steinke, C. G. R. Geddes, N. H. Matlis, B. H. Shaw, A. J. Gonsalves, J. V. Huijts, K. Nakamura, J. Daniels, C. B. Schroeder, C. Benedetti, E. Esarey, S. S. Bulanov, N. A. Bobrova, P. V. Sasorov, and W. P. Leemans, Active plasma lensing for relativistic laser-plasma-accelerated electron beams, Phys. Rev. Lett. **115**, 184802 (2015).

[63] M. Migliorati, A. Bacci, C. Benedetti, E. Chiadroni, M. Ferrario, A. Mostacci, L. Palumbo, A. R. Rossi, L. Serafini, and P. Antici, Intrinsic normalized emittance growth in laser-driven electron accelerators, Phys. Rev. ST Accel. Beams **16**, 011302 (2013).

[64] C. A. Lindstrøm, Staging of plasma-wakefield accelerators, Phys. Rev. Accel. Beams **24**, 014801 (2021).

[65] A. Ferran Pousa, R. Assmann, and A. Martinez de la Ossa, Wake-t: a fast particle tracking code for plasma-based accelerators, J. Phys. Conf. Ser. **1350**, 012056 (2019).

[66] R. Lehe, M. Kirchen, I. A. Andriyash, B. B. Godfrey, and J.-L. Vay, A spectral, quasi-cylindrical and dispersion-free particle-in-cell algorithm, Comput. Phys. Commun. **203**, 66 (2016).

[67] I. Agapov, G. Geloni, S. Tomin, and I. Zagorodnov, Ocelot: A software framework for synchrotron light source and fel studies, Nucl. Instrum. Methods Phys. Res. A **768**, 151 (2014).

[68] S. Hudson, J. Larson, J.-L. Navarro, and S. M. Wild, libensemble: A library to coordinate the concurrent evaluation of dynamic ensembles of calculations, IEEE Trans. Parallel Distrib. Syst. **33**, 977 (2022).

[69] See supplemental material at [] for additional details about the simulated setups and simulation parameters, which includes refs. [74–77].

[70] M. Santarsiero, D. Aiello, R. Borghi, and S. Vicalvi, Focusing of axially symmetric flattened gaussian beams, J. Mod. Opt. **44**, 633 (1997).

[71] M. Kirchen, Ph.D. thesis, Universität Hamburg (2021).

[72] F. Wu, Z. Zhang, X. Yang, J. Hu, P. Ji, J. Gui, C. Wang, J. Chen, Y. Peng, X. Liu, Y. Liu, X. Lu, Y. Xu, Y. Leng, R. Li, and Z. Xu, Performance improvement of a 200tw/1hz ti:sapphire laser for laser wakefield electron accelerator, Opt. Laser Technol. **131**, 106453 (2020).

[73] Jülich Supercomputing Centre, JUWELS: Modular Tier-0/1 Supercomputer at the Jülich Supercomputing Centre, Journal of large-scale research facilities **5**, 10.17815/jlsrf-5-171 (2019).

[74] J.-L. Vay, Noninvariance of space- and time-scale ranges under a lorentz transformation and the implications for the study of relativistic interactions, Phys. Rev. Lett. **98**, 130405 (2007).

[75] J.-L. Vay, C. G. R. Geddes, E. Esarey, C. B. Schroeder, W. P. Leemans, E. Cormier-Michel, and D. P. Grote, Modeling of 10 gev-1 tev laser-plasma accelerators using lorentz boosted simulations, Phys. Plasmas **18**, 123103 (2011).

[76] R. Lehe, M. Kirchen, B. B. Godfrey, A. R. Maier, and J.-L. Vay, Elimination of numerical cherenkov instability in flowing-plasma particle-in-cell simulations by using galilean coordinates, Phys. Rev. E **94**, 053305 (2016).

[77] M. Kirchen, R. Lehe, B. B. Godfrey, I. Dornmair, S. Jalas, K. Peters, J.-L. Vay, and A. R. Maier, Stable discrete representation of relativistically drifting plasmas, Phys. Plasmas **23**, 100704 (2016).